Hindawi
Journal of Electrical and Computer Engineering
Volume 2018, Article ID 9684629, 9 pages
https://doi.org/10.1155/2018/9684629

Research Article

Extraction of Earth Surface Texture Features from Multispectral Remote Sensing Data

Zhenxing Zhang,[1] Feng Gao,[1] Bin Ma,[2] and Zhiqiang Zhang[3]

[1]*College of Automation, Harbin Engineering University, Harbin 150001, China*
[2]*China Ship Development and Design Center, Wuhan, China*
[3]*92730 Army, Sanya 572016, China*

Correspondence should be addressed to Feng Gao; gaofeng19@hrbeu.edu.cn

Received 12 December 2017; Accepted 18 March 2018; Published 25 October 2018

Academic Editor: Jose R. C. Piqueira

Earth surface texture features referring to as visual features of homogeneity in remote sensing images are very important to understand the relationship between surface information and surrounding environment. Remote sensing data contain rich information of earth surface texture features (image gray reflecting the spatial distribution information of texture features, for instance). Here, we propose an efficient and accurate approach to extract earth surface texture features from remote sensing data, called gray level difference frequency spatial (GLDFS). The gray level difference frequency spatial approach is designed to extract multiband remote sensing data, utilizing principle component analysis conversion to compress the multispectral information, and it establishes the gray level difference frequency spatial of principle components. In the end, the texture features are extracted using the gray level difference frequency spatial. To verify the effectiveness of this approach, several experiments are conducted and indicate that it could retain the coordination relationship among multispectral remote sensing data, and compared with the traditional single-band texture analysis method that is based on gray level co-occurrence matrix, the proposed approach has higher classification precision and efficiency.

1. Introduction

Remote sensing technology can extract high resolution regional marine environmental information in time, especially for the complex sea area. Multispectral remote sensing data reflects the interested target or regional radiation characteristics through the electromagnetic spectrum of multiband, and it has the advantages of wide range, multiphase, multiband, and high resolution. Remote sensing image could enrich the spectral characteristics of landmark and find out more detailed information, such as the structure, shape, and texture. However, in virtue of the fact that same objects possess different spectral and different objects share same spectral, the applications of remote sensing data would be serious restricted if only spectral information is taken into consideration. The earth surface texture is a good solution to the problem because of the stability characteristics [1].

The classical texture extraction and analytic approaches include gray level co-occurrence matrix method [2, 3], wavelet analysis method [4, 5], Gabor spectrum method [6], and so forth. While all these methods could only be applied to analyze the information of single band in remote sensing images, for multispectral remote sensing data, all the bands should be processed separately, which would decrease the extraction efficiency badly.

Because of the geometric characteristics of the surface object, it has a unique texture features on the remote sensing images. So, the different surface objects can be extracted through the texture features. This paper utilizes gray level difference frequency spatial to extract texture features of multiband remote sensing data. We firstly conduct principal component analysis (PCA) on the eight bands of Worldview-II multispectral images and compress these data on basis of guaranteeing against loss of spectral information. Make gray difference statistics on the compressed principle components and establish the gray level difference frequency spatial. In the experiments, the gray level difference frequency spatial is used to extract texture features, and a comparison with Gray Level

Co-occurrence Matrix (GLCM) is made. The experimental results indicate that the gray level difference frequency spatial has higher classification accuracy and efficiency.

2. Worldview-II Multispectral Remote Sensing Data

Worldview-II is one of the highest resolution remote sensing satellites, and it has the highest spatial resolution (0.46 m in the panchromatic band and 1.84 m in the multispectral bands). It provides high resolution multispectral data with eight bands, which include four conventional bands (red, green, blue, and near-infrared 1) and four characteristic bands (coastal, yellow, red edge, and near-infrared 2). The data analyzed in this paper are Worldview-II multispectral remote sensing image of the Sea Islands; the texture features of eight bands are extracted. Firstly, we calibrate the data and get the radiance data. Secondly, atmospheric correction is conducted to eliminate the influence of atmosphere and illumination, and the actual reflectance of surface objects is obtained. Finally, we make orthorectification on the data through a few control points, thus eliminating the geometric distortion.

3. Compression of Multispectral Remote Sensing Data

Principal component analysis could project the high dimensional data onto a low-dimensional space. It takes the variance in size as the evaluation standard of information quantity; the greater the variance, the more information it provides [7, 8]. On the premise of keeping useful information of multispectral remote sensing data, principal component analysis could reduce the correlation and redundant information in order to compress multispectral remote sensing data. We transform Worldview-II multispectral remote sensing data into a column vector $\mathbf{W}$ as follows:

$$\mathbf{W} = \left[\, \mathbf{w}_1,\ \mathbf{w}_2,\ \cdots,\ \mathbf{w}_n \,\right]^{\mathrm{T}}, \quad (n = 1, 2, \cdots, 8). \tag{1}$$

Principal component analysis makes a combination of $\mathbf{W}$ through linear transformation and guarantees that $\mathbf{P}$ has the largest variance after transformation, as shown in the following equation:

$$\mathbf{P} = \mathbf{L}^{\mathrm{T}}\mathbf{W}, \tag{2}$$

where $\mathbf{L} = (l_1, l_2, l_3, \cdots, l_n)$ is the m-dimensional space to be determined and $\mathbf{R}$ is the covariance matrix of $\mathbf{W}$, thereby, the variance of $\mathbf{P}$ could be computed as follows:

$$D(\mathbf{P}) = \mathbf{L}^{\mathrm{T}}\mathbf{R}\mathbf{L}. \tag{3}$$

Thereby, solving the maximum value of $D(\mathbf{P})$ is equal to seeking the vector $\mathbf{L}$ that makes $D(\mathbf{P})$ the largest. The length $\mathbf{L}$ is limited to unit length, and then the question is converted to

$$\begin{aligned} &\max \quad D(\mathbf{P}) = \mathbf{L}^{\mathrm{T}}\mathbf{R}\mathbf{L}, \\ &\text{s.t.} \quad \mathbf{L}^{\mathrm{T}}\mathbf{L} = 1. \end{aligned} \tag{4}$$

In last equation, the covariance matrix $\mathbf{R}$ could be expressed as follows:

$$\mathbf{R} = \Gamma \mathrm{diag}(\lambda_1, \cdots \lambda_{\mathrm{n}})\Gamma^{\mathrm{T}}, \tag{5}$$

where $\lambda_1, \cdots \lambda_{\mathrm{n}}$ is the characteristic value of $\mathbf{R}$ and $\lambda_1 \geq \lambda_2 \geq \cdots \geq \lambda_n$ is satisfied. $\Gamma = (\mathbf{a}_1, \mathbf{a}_2, \cdots, \mathbf{a}_n)$, where $\mathbf{a}_1$, $\mathbf{a}_2, \cdots, \mathbf{a}_n$ is the eigenvector corresponding to the unit orthogonal eigenvectors. Let $\mathbf{a} \in \mathbf{R}^n$ and multiplying Equation (5) with $\mathbf{a}^{\mathrm{T}}$ and $\mathbf{a}$ on the left and right side separately, we get

$$\mathbf{a}^{\mathrm{T}}\mathbf{R}\mathbf{a} = \mathbf{a}^{\mathrm{T}}\Gamma \mathrm{diag}(\lambda_1, \cdots \lambda_{\mathrm{n}})\Gamma^{\mathrm{T}}\mathbf{a}. \tag{6}$$

Let $k = \Gamma^{\mathrm{T}}\mathbf{a}$, then $\mathbf{a}^{\mathrm{T}}\mathbf{a} = \mathbf{k}^{\mathrm{T}}\mathbf{k}$; Equation (6) satisfies

$$\begin{aligned} \mathbf{a}^{\mathrm{T}}\mathbf{R}\mathbf{a} &= \mathbf{k}^{\mathrm{T}}\mathrm{diag}(\lambda_1, \cdots \lambda_{\mathrm{n}})\mathbf{k} = \lambda_1\mathbf{k}_1^2 + \lambda_2\mathbf{k}_2^2 + \cdots + \lambda_n\mathbf{k}_n^2 \\ &\leq \lambda_1\left(\mathbf{k}_1^2 + \mathbf{k}_2^2 + \cdots + \mathbf{k}_n^2\right). \end{aligned} \tag{7}$$

Equation (4) can be rewritten as follows:

$$\max_{\mathbf{L}^{\mathrm{T}}\mathbf{L}=1} \mathbf{L}^{\mathrm{T}}\mathbf{R}\mathbf{L} = \max_{\mathbf{k}^{\mathrm{T}}\mathbf{k}=1}\left(\lambda_1\mathbf{k}_1^2 + \lambda_2\mathbf{k}_2^2 + \cdots + \lambda_n\mathbf{k}_n^2\right) \leq \lambda_1. \tag{8}$$

If $\mathbf{a} = \mathbf{a}_1$, then $\mathbf{a}_1^{\mathrm{T}}\mathbf{R}\mathbf{a}_1 = \lambda_1$, which indicates that the maximum value of $\mathbf{L}^{\mathrm{T}}\mathbf{R}\mathbf{L}$ is at the point of $\mathbf{a}_1$ under the condition of $\mathbf{L}^{\mathrm{T}}\mathbf{L} = 1$, thereby the first PCA principle component could be expressed as $\mathbf{p}_1 = \mathbf{a}_1^{\mathrm{T}}\mathbf{W}$. The contribution rate reflects the information quantity contained in each principle component, and the contribution rate of the i-th principal component could be computed as follows:

$$\frac{\lambda_i}{\mathrm{tr}(\mathbf{R})} = \frac{\lambda_i}{\sum_{k=1}^{n}\lambda_k}. \tag{9}$$

The cumulative contribution rate of the first l principal components is as follows:

$$\frac{\sum_{i=1}^{l}\lambda_i}{\sum_{k=1}^{n}\lambda_k}. \tag{10}$$

The contribution rate indicates the ability that principle components reflect $\mathbf{W}$. It determines the number of principal components after compression of multispectral remote sensing data.

4. Texture Features Extraction from Multispectral Remote Sensing Data

4.1. Gray Level Co-Occurrence Matrix. Gray Level Co-occurrence Matrix is the most direct and simplest texture analysis approach, which considers the spatial structure of remote sensing images [9]. It describes the image texture through the two-order combined conditional probability density among image pixels [10]. Assume the remote sensing image is of size $M \times N$; the gray level is L; the distance between two pixels is d; the angle is θ; the gray levels are separately i and j; the times that these two pixels appear simultaneously is $\mathbf{P}(i, j, d, \theta)$ which could be expressed as follows:

$$\begin{aligned} \mathbf{P}(i, j, d, \theta) = \{[(x_1, y_1), (x_2, y_2)] \mid f(x_1, y_1) = i, f(x_2, y_2) \\ = j; x_1, x_2 = 1, 2, \cdots m; y_1, y_2 = 1, 2, \cdots n;\}, \end{aligned} \tag{11}$$

Where m and n represent the number of remote sensing image pixels in a row and a column; $i, j = 1, 2, \cdots L$, x_1, y_1, x_2, y_2 are the pixel coordinates in the image. Figure 1 shows the spatial sketch map of GLCM. If the remote sensing image has L picture gray levels, the size of the gray level co-occurrence matrix is $L \times L$, d represents the distance of two pixels in the remote sensing image, θ represents the angle between the connection line of the two pixels and horizontal direction, and it is usually set as 0°, 45°, 90°, and 135°. The element at the a-th row and b-th column in $\mathbf{P}(i, j, d, \theta)$ represents the appearance times of all the pixel couples that are δ apart from each other in the θ direction, with gray values i and j, respectively. d is related to the image, the step is usually set as $\delta = 1$, and the central pixel to be operated and compared with the directly adjacent pixel.

4.2. Establishment of the Gray Level Difference Frequency Spatial. Gray level difference frequency spatial is proposed as a texture extraction approach for the multiprinciple component, which is based on the Gray Level Co-occurrence Matrix. Assume the gray level of primary gradient remote sensing image is g; firstly, iterate the principle components' remote sensing image with a rectangular window which is of size $m \times n$. Assume $L_m = \{1, 2, \cdots, m\}$ and $L_n = \{1, 2, \cdots, n\}$ are separately the horizontal and vertical spatial domains of the window and $G = \{0, 1, \cdots, g-1\}$ is the gray level. $L_n \times L_m$ is the windows' pixel set with ranking sequence in the row and column, specifying I as the conversion formula of pixels in $L_n \times L_m$ to G:

$$I : L_n \times L_m \longrightarrow G. \tag{12}$$

In different windows of principle components' image, the appearance probability of the pixel couples with distance d, direction θ, and gray level difference Δ composing the GLDFS and it is named $\mathbf{P}$, in which $(m1_{Pi}, n1_{Pi})$, $(m2_{Pi}, n2_{Pi})$ are coordinates of two pixels in the $i-th$ principal component $L_n \times L_m$; $I(m1_{Pi}, n1_{Pi})$, $I(m2_{Pi}, n2_{Pi})$ are gray levels corresponding to the two pixels; and $(m2_{Pi}, n2_{Pi})$ locates in the θ direction of $(m1_{Pi}, n1_{Pi})$ with distance d. The two pixel gray level's difference is expressed as follows:

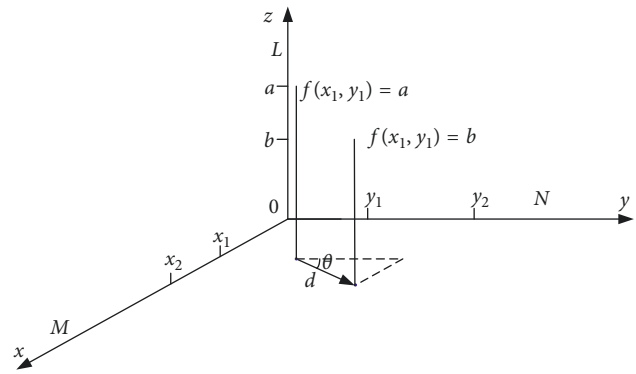

Figure 1: The space description of the GLCM.

$$\Delta_i = \left| I\left(m1_{Pi}, n1_{Pi}\right) - I\left(m2_{Pi}, n2_{Pi}\right) \right|, \tag{13}$$

where $\Delta_i \in [0, g-1]$. Make statistics of the gray level difference in each principal component and map the result to k-dimensional space according to the distance d and direction θ. The coordinates of the spatial points are $(\Delta_1, \Delta_2, \cdots, \Delta_k)$, and k is the number of the principle components' remote sensing images. Meanwhile, make statistics for each principal component at the four directions 0°, 45°, 90°, and 135°, thereby generating four n-dimensional spaces, and # indicates the number of the elements in the space; the statistical methods are as follows:

$$\mathbf{P}^k\left(\Delta_1, \Delta_2, \cdots \Delta_k, d, 0^0\right) = \#\left\{ \begin{array}{l|l} (m1_{P1}, n1_{P1}), (m2_{P1}, n2_{P1}) \in (L_n \times L_m) \times (L_n \times L_m) & m1_{P1} - m2_{P1} = 0, \left|n1_{P1} - n2_{P1}\right| = d,\ \left|I(m1_{P1}, n1_{P1}) - I(m2_{P1}, n2_{P1})\right| = \Delta_1 \\ (m1_{P2}, n1_{P2}), (m2_{P2}, n2_{P2}) \in (L_n \times L_m) \times (L_n \times L_m) & m1_{P2} - m2_{P2} = 0, \left|n1_{P2} - n2_{P2}\right| = d,\ \left|I(m1_{P2}, n1_{P2}) - I(m2_{P2}, n2_{P2})\right| = \Delta_2 \\ \vdots & \vdots \\ (m1_{Pk}, n1_{Pk}), (m2_{Pk}, n2_{Pk}) \in (L_n \times L_m) \times (L_n \times L_m) & m1_{Pk} - m2_{Pk} = 0, \left|n1_{Pk} - n2_{Pk}\right| = d,\ \left|I(m1_{Pk}, n1_{Pk}) - I(m2_{Pk}, n2_{Pk})\right| = \Delta_k \end{array} \right\}, \tag{14}$$

$$\mathbf{P}^n\left(\Delta_1, \Delta_2, \cdots \Delta_k, d, 45^0\right) = \#\left\{ \begin{array}{l|l} (m1_{P1}, n1_{P1}), (m2_{P1}, n2_{P1}) \in (L_n \times L_m) \times (L_n \times L_m) & (m1_{P1} - m2_{P1} = d, n1_{P1} - n2_{P1} = -d) \text{ or } (m1_{P1} - m2_{P1} = -d, n1_{P1} - n2_{P1} = d),\ \left|I(m1_{P1}, n1_{P1}) - I(m2_{P1}, n2_{P1})\right| = \Delta_1 \\ (m1_{P2}, n1_{P2}), (m2_{P2}, n2_{P2}) \in (L_n \times L_m) \times (L_n \times L_m) & (m1_{P2} - m2_{P2} = d, n1_{P2} - n2_{P2} = -d) \text{ or } (m1_{P2} - m2_{P2} = -d, n1_{P2} - n2_{P2} = d),\ \left|I(m1_{P2}, n1_{P2}) - I(m2_{P2}, n2_{P2})\right| = \Delta_2 \\ \vdots & \vdots \\ (m1_{Pk}, n1_{Pk}), (m2_{Pk}, n2_{Pk}) \in (L_n \times L_m) \times (L_n \times L_m) & (m1_{Pk} - m2_{Pk} = d, n1_{Pk} - n2_{Pk} = -d) \text{ or } (m1_{Pk} - m2_{Pk} = -d, n1_{Pk} - n2_{Pk} = d)\ \left|I(m1_{Pk}, n1_{Pk}) - I(m2_{Pk}, n2_{Pk})\right| = \Delta_k \end{array} \right\}, \tag{15}$$

$$\mathbf{P}^k\left(\Delta_1, \Delta_2, \cdots \Delta_k, d, 90^0\right) = \#\left\{ \begin{array}{l|l} (m1_{P1}, n1_{P1}), (m2_{P1}, n2_{P1}) \in (L_n \times L_m) \times (L_n \times L_m) & \left|m1_{P1} - m2_{P1}\right| = d, n1_{P1} - n2_{P1} = 0,\ \left|m1_{P2} - m2_{P2}\right| = d, n1_{P2} - n2_{P2} = 0 \\ (m1_{P2}, n1_{P2}), (m2_{P2}, n2_{P2}) \in (L_n \times L_m) \times (L_n \times L_m) & \left|m1_{P2} - m2_{P2}\right| = d, n1_{P2} - n2_{P2} = 0,\ \left|I(m1_{P2}, n1_{P2}) - I(m2_{P2}, n2_{P2})\right| = \Delta_2 \\ \vdots & \vdots \\ (m1_{Pk}, n1_{Pk}), (m2_{Pk}, n2_{Pk}) \in (L_n \times L_m) \times (L_n \times L_m) & \left|m1_{Pk} - m2_{Pk}\right| = d, n1_{Pk} - n2_{Pk} = 0,\ \left|I(m1_{Pk}, n1_{Pk}) - I(m2_{Pk}, n2_{Pk})\right| = \Delta_k \end{array} \right\}, \tag{16}$$

$$\mathbf{P}^n\left(\Delta_1, \Delta_2, \cdots \Delta_k, d, 135^0\right) = \#\left\{ \begin{array}{l|l} (m1_{P1}, n1_{P1}), (m2_{P1}, n2_{P1}) \in (L_n \times L_m) \times (L_n \times L_m) & (m1_{P1} - m2_{P1} = d, n1_{P1} - n2_{P1} = d) \text{ or } (m1_{P1} - m2_{P1} = -d, n1_{P1} - n2_{P1} = -d),\ \left|I(m1_{P1}, n1_{P1}) - I(m2_{P1}, n2_{P1})\right| = \Delta_1 \\ (m1_{P2}, n1_{P2}), (m2_{P2}, n2_{P2}) \in (L_n \times L_m) \times (L_n \times L_m) & (m1_{P2} - m2_{P2} = d, n1_{P2} - n2_{P2} = d) \text{ or } (m1_{P2} - m2_{P2} = -d, n1_{P2} - n2_{P2} = -d),\ \left|I(m1_{P2}, n1_{P2}) - I(m2_{P2}, n2_{P2})\right| = \Delta_2 \\ \vdots & \vdots \\ (m1_{Pk}, n1_{Pk}), (m2_{Pk}, n2_{Pk}) \in (L_n \times L_m) \times (L_n \times L_m) & (m1_{Pk} - m2_{Pk} = d, n1_{Pk} - n2_{Pk} = d) \text{ or } (m1_{Pk} - m2_{Pk} = -d, n1_{Pk} - n2_{Pk} = -d)\ \left|I(m1_{Pk}, n1_{Pk}) - I(m2_{Pk}, n2_{Pk})\right| = \Delta_k \end{array} \right\}. \tag{17}$$

4.3. Texture Features' Description of the Gray Level Difference Frequency Spatial. Haralick proposed Gray Level Co-occurrence Matrix 14 properties to describe the image's texture features, and Sor proposed Gray Level Co-occurrence Matrix 10 properties aiming at the SAR images [11]. But some properties are relevant, resulting in information redundancy; besides, part of properties is not suitable for analysis of remote sensing images' texture features [12–14]. This paper makes analysis of seven texture features with GLDFS and could be computed as follows:

(1) Energy:

$$T_1 = \sum_{\Delta_1} \sum_{\Delta_2} \cdots \sum_{\Delta_n} \{\mathbf{P}^n(\Delta_1, \Delta_2, \cdots, \Delta_n)\}^2. \tag{18}$$

(2) Entropy:

$$T_2 = -\sum_{\Delta_1} \sum_{\Delta_2} \cdots \sum_{\Delta_n} \mathbf{P}^n(\Delta_1, \Delta_2, \cdots, \Delta_n) \cdot \log(\mathbf{P}^n(\Delta_1, \Delta_2, \cdots, \Delta_n)). \tag{19}$$

(3) Autocorrelation:

$$T_3 = \sum_{\Delta_1} \sum_{\Delta_2} \cdots \sum_{\Delta_n} (\Delta_1, \Delta_2, \cdots, \Delta_n)\mathbf{P}^n(\Delta_1, \Delta_2, \cdots, \Delta_n). \tag{20}$$

(4) Correlation:

$$T_4 = \sum_{\Delta_1} \sum_{\Delta_2} \cdots \sum_{\Delta_n} (\Delta_1, \Delta_2, \cdots, \Delta_n)\mathbf{P}^n \cdot (\Delta_1, \Delta_2, \cdots, \Delta_n) \quad \frac{-\mu_{\Delta_1}\mu_{\Delta_2}\cdots\mu_{\Delta_n}}{\sigma_{\Delta_1}\sigma_{\Delta_2}\cdots\sigma_{\Delta_n}}. \tag{21}$$

(5) Highlight degree of clustering:

$$T_5 = \sum_{\Delta_1} \sum_{\Delta_2} \cdots \sum_{\Delta_n} \left(\Delta_1 + \Delta_2 + \cdots \Delta_n - \mu_{\Delta_1}\mu_{\Delta_2}\cdots\mu_{\Delta_n}\right)^3 \mathbf{P}^n \cdot (\Delta_1, \Delta_2, \cdots, \Delta_n). \tag{22}$$

(6) Dark degree of clustering:

$$T_6 = \sum_{\Delta_1} \sum_{\Delta_2} \cdots \sum_{\Delta_n} \left(\Delta_1 + \Delta_2 + \cdots \Delta_n - \mu_{\Delta_1}\mu_{\Delta_2}\cdots\mu_{\Delta_n}\right)^4 \mathbf{P}^n \cdot (\Delta_1, \Delta_2, \cdots, \Delta_n). \tag{23}$$

(7) The maximum similarity:

$$T_7 = \underset{\Delta_1, \Delta_2, \cdots, \Delta_n}{\mathrm{MAX}} \mathbf{P}^n(\Delta_1, \Delta_2, \cdots, \Delta_n) \tag{24}$$

The energy, entropy, autocorrelation, and correlation are the extentions of Haralick's method in high-dimensional space, and the maximum similarity is generalization of Soh's method, the highlight degree, and the dark degree of clustering, which are the simulation calculations of human perception.

5. Analysis of Experimental Results

The experiment data are based on the multispectral remote sensing data of 8 different bands, which were recorded by Worldview-II on 8th April, 2009. In order to ensure the same landform features, the reef selected by the experiment is uncovered with plants consisting of sedimentary and metamorphic rocks. Gray value variance has a regular pattern when counted on space and texture feature shows up with strong intensify as well, so this paper tests and verifies the gray level difference frequency spatial texture feature extracting method through the classification of landform and compares it with the Gray Level Co-occurrence Matrix. The gray level difference frequency spatial and Gray Level Co-occurrence Matrix choose worldview-II remote sensing data of the same region which cohere well, and thus the comparability of the experiment data is assured. Experimental classification uses SVM, which is based on structural risk minimization principle. SVM is a better solution to small samples and nonlinear problems.

5.1. The Experimental Data Compression. PCA is applied to compression of 8 different bands of Worldview-II multispectral remote sensing data. In this paper, the first three principal components are derived as the feature of the gray level difference frequency spatial texture feature. Figure 2 shows the contribution rate as well as the cumulative contribution rate of each main component of the Worldview-II 8-band multispectral data after principal component analysis transform. Figure 3 shows the three principal component image data after principal component analysis transformation and compression. Figure 3(a) shows the first principal component, and the contribution rate is 74.12%. Figure 3(b) shows the second principal component, and the contribution rate is 22.16%. Figure 3(c) shows the third principal component, and the contribution rate is 2.73%.

5.2. The Classification and Analysis of Sample Data Experiment. Deriving the texture features of the three principal components after being compressed with the gray level difference frequency spatial and deriving the texture features of the four regular bands and four special bands which are compared separately with Gray Level Co-occurrence Matrix, the distance d of both methods is 1; merely comparing the gray-scale changes of the adjacent pixel, the window size is 13×13. Features including energy, self-correlation, correlation, cluster dark, and maximum self-similarity are selected; the sample size is 1350 among which the reef, sea, and foam samples are 350 separately. The SVM pattern is applied for the purpose of dividing the data into three. The result of landmark feature classification with the gray level difference frequency spatial and Gray Level Co-occurrence Matrix are shown in Tables 1 and 2. The recognition rate is based on the typical testing samples randomly selected from the samples including reef, sea, and foam data. Calculating the percentage of correct

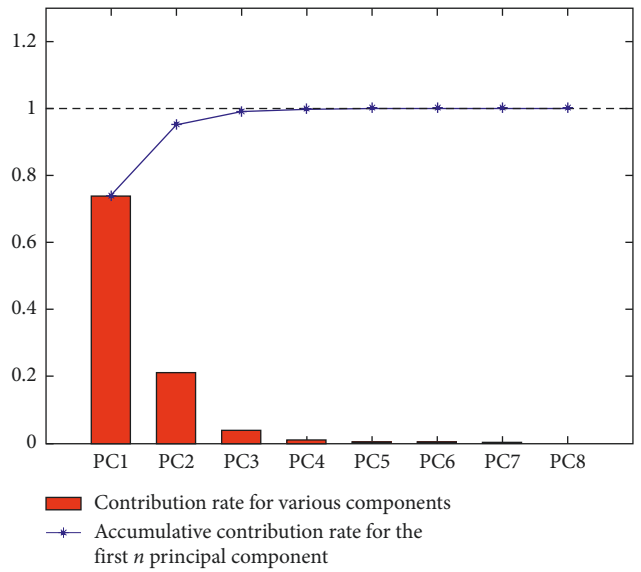

Figure 2: The contribution rate and the cumulative contribution rate of each principal component.

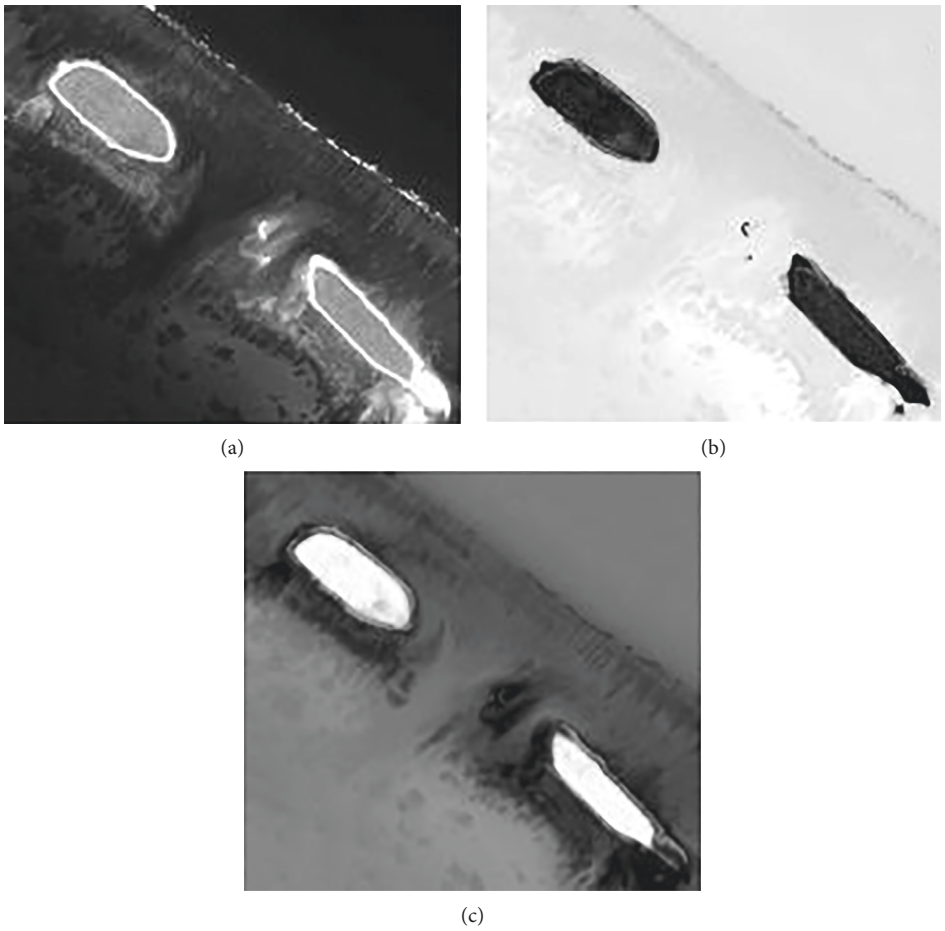

Figure 3: Image after PCA transformation and compression: (a) first principal component, (b) second principal component, and (c) third principal component.

identification number for each landmark class with its corresponding total samples, the average value is the right recognition number of the three types of landmarks with the gross sample number. It can be figured out that the gray level difference frequency spatial is capable of dealing with three types of landmark features at the same time and has better

Table 1: The recognition rate of GLDFS and GLCM of conventional bands.

Recognition rate (%)	Blue band	Green band	Red band	Near-infrared 1 band	Principal component data
	GLCM of conventional bands				GLDFS
Reef	60.2	64.6	62.9	79.8	89.3
Seawater	72.3	50.3	34.2	18.9	92.8
Foam	81.2	79.4	49.6	89.3	70.7
Average	65.4	71.3	30.9	62.4	85.9

Table 2: The recognition rate of GLDFS and GLCM of characteristic bands.

Recognition rate (%)	Coastal band	Yellow band	Infrared band	Near-infrared 2 band	Principal component data
	GLCM of characteristic bands				GLDFS
Reef	70.1	64.3	91.4	95.4	93.1
Sea	69.3	30.4	39.8	2.8	94.5
Foam	74.9	49.8	7.9	93.8	69.8
Average	63.2	55.2	54.6	71.2	83.6

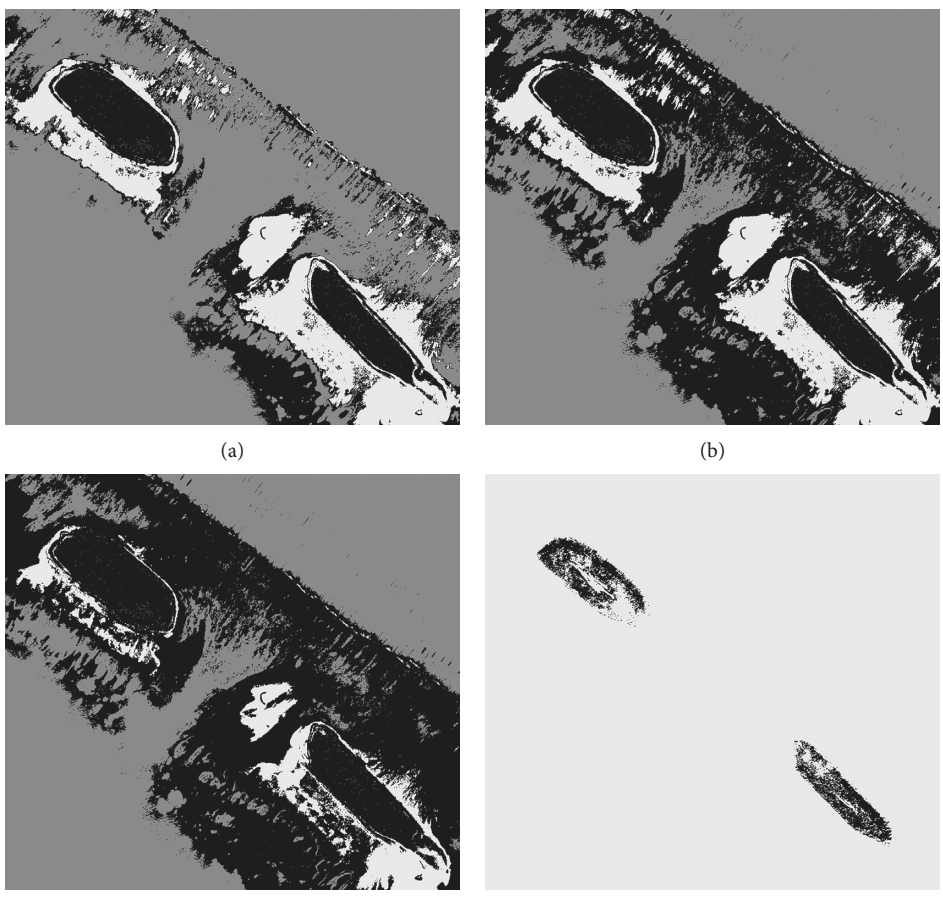

(a) (b) (c) (d)

Figure 4: Continued.

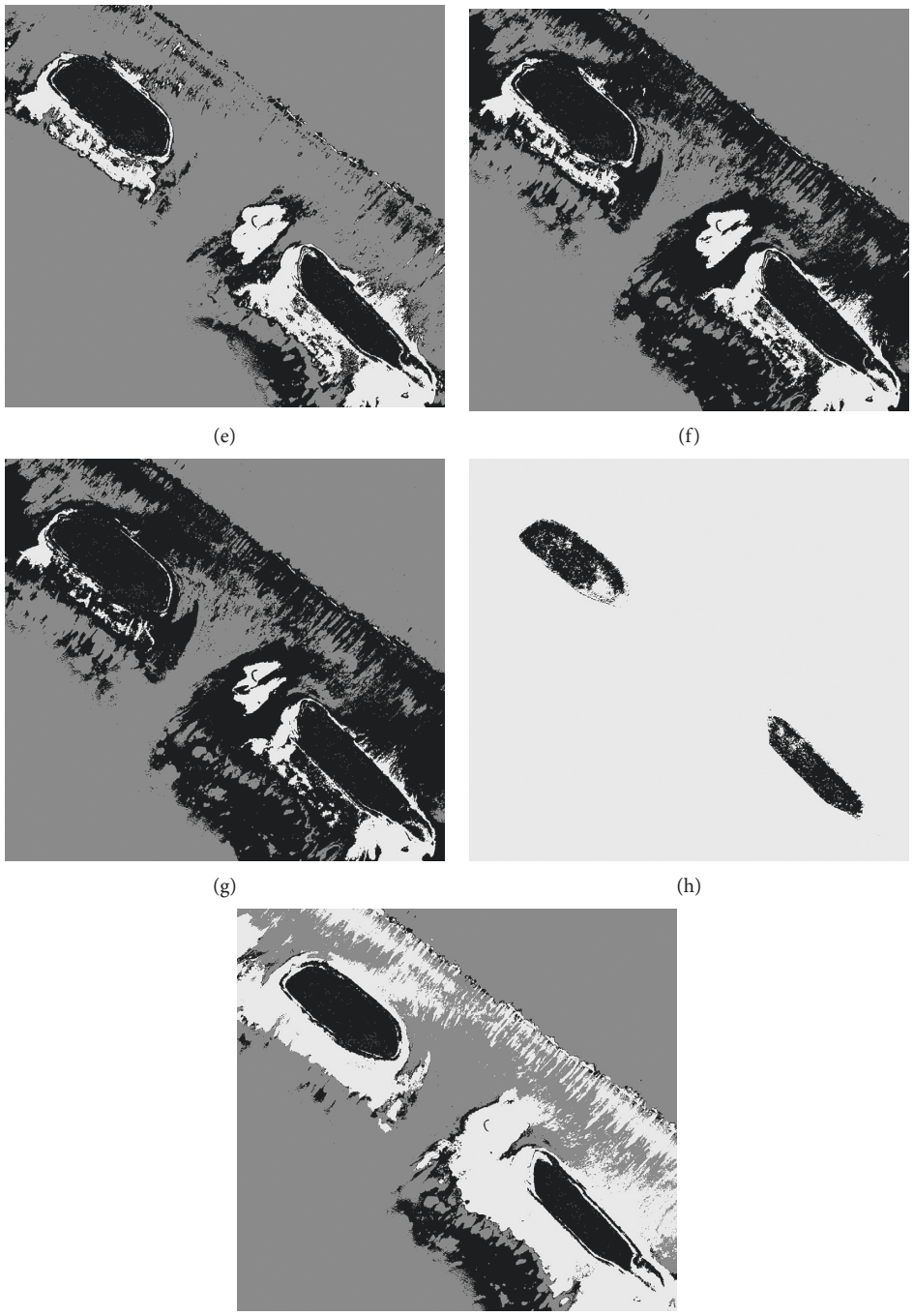

(e) (f) (g) (h) (i)

Figure 4: The classification processing results of GLDFS in conventional bands and characteristic bands and GLCM in principal component data: (a) blue band, (b) green band, (c) red band, (d) near-infrared 1 band, (e) coastal band, (f) yellow band, (g) infrared band, (h) near-infrared 2 band, and (i) principal component data.

recognition efficiency and quality than traditional Gray Level Co-occurrence Matrix.

The classification using the gray level difference frequency spatial and the classification using Gray Level Co-occurrence Matrix in conventional bands and characteristic bands of processing results about principal component data can be seen from Figure 4. In Figure 4, black indicates the reef, dark gray indicates foam, and light gray indicates sea. Figures 4(a)–4(d) are the classification result of conventional bands of the Gray Level Co-occurrence Matrix. Figures 4(e)–4(h) are the classification result of characteristic bands of the Gray Level Co-occurrence Matrix. Figure 4(i) is the classification result of the principal component data of the gray level difference frequency spatial. This paper presents a method named the gray level difference frequency spatial for the principal components data processing and has

Table 3: The comparision of SVM multisclassification efficiency.

Experimental data	Conventional bands	Special bands	Principal component data
Extraction method of input variables	GLCM		GLDFS
Recognition rate of reef (%)	93.2	87.3	91.6
Recognition rate of seawater (%)	93.9	89.7	96.1
Recognition rate of foam (%)	81.6	74.3	76.1
Recognition rate of average (%)	78.2	86.3	83.9
Spending of time (s)	93	89	45

a better classification results with three kinds of surface features. The method of Gray Level Co-occurrence Matrix has poor identification with reef when it is processing blue bands and coastal bands, and some island and reef are identified as foam mistakenly; when green bands and yellow bands is processing, the identification to seawater is poor, some seawater is identified as reef and island mistakenly; when red band and red edge band are processing, the identification to seawater and foam is poor, some seawater and foam is identified as reef and island mistakenly; when No. 1 and No. 2 bands of near-infrared are processing, seawater is identified as foam. The method of Gray Level Co-occurrence Matrix has high recognition to some landmark, but for the multilandmarks of multispectral remote sensing data, it cannot be guaranteed to have higher recognition rate in classification. If a variety of surface landmarks is classified, the single-band data need to be processed separately. In the experiment, texture features are extracted from the conventional band and special band data using Gray Level Co-occurrence Matrix method and from the principal component data using gray level difference frequency spatial method. The extracted results are processed and used as SVM input variables of multilandmark classification. Finally, the classification time consumption is compared and analyzed. The efficiency of texture feature extracted by two methods using SVM classification is as shown in Table 3, and the results show that the gray level difference frequency spatial to the main component of compressed data has better efficiency in ensuring a higher recognition rate, but takes long time. The main reason is that the conventional band and special bands contain four bands of data; Gray Level Co-occurrence Matrix requires processing individual band and makes the results of 4 bands as SVM input variables to multilandmark classification. Due to the increased dimension of the input variables, the efficiency of calculation of SVM is reduced and the classification time becomes longer.

6. Conclusions and Discussions

According to the Worldview-II multispectral remote sensing data, this paper proposed a texture feature method based on gray-scale difference in space-frequency. This method compresses the multispectral remote sensing data after having it disposed, carries out gray-scale statistic on the main components after the compression process, and builds the gray-scale frequency difference space model. The method is validated by taking the data collected by Worldview-II. From the results, it can be seen that the gray level difference frequency spatial can extract texture features and recognize and classify multiband, multi-landmark, and multi-spectral remote sensing data at the same time and has an advantage over tradition Gray Level Co-occurrence Matrix on consideration of both recognition efficiency and quality.

Conflicts of Interest

The authors declare that they have no conflicts of interest.

Acknowledgments

This work was funded by the National Key Research and Development Project of China (2017YFC1404100, 2017YFC1404102).

References

[1] J. Feng and N. Shu, "A novel texture feature extraction of hyperspectral," *Journal of WuHan University of Technology*, vol. 31, no. 3, pp. 11–17, 2009.

[2] R. M. Haralick, K. Shanmugam, and I. H. Dinstein, "Textural features for image classification," *IEEE Transactions on Systems, Man, and Cybernetics*, vol. 3, no. 6, pp. 610–621, 1973.

[3] G. N. Srinivasa and G. Shobba, "Statstical texture analysis," *Proceedings of World Academy of Science, Engineering and Technology*, vol. 11, pp. 196–201, 2006.

[4] C. S. Lu, P. C. Chung, and C. F. Chen, "Unsupervised texture segmentation via wavelet transform," *Pattern recognition*, vol. 30, no. 5, pp. 729–742, 1997.

[5] M. K. Bashar, T. Matsumoto, and N. Ohnishi, "Wavelet transform-based locally orderless images for texture segmentation," *Pattern Recognition Letters*, vol. 24, no. 15, pp. 2633–2650, 2003.

[6] A. K. Jain and F. Farshid, "Unsupervised texture segmentation using Gabor Filters," *Pattern recognition*, vol. 24, no. 12, pp. 1167–1186, 1991.

[7] A. Kaarna, "Integer PCA and wavelet transforms for multispectral image compression," in *Proceedings of International Geoscience and Remote Sensing Symposium*, pp. 1853–1855, Sydney, Australia, July 2001.

[8] C. Jutten and J. Herault, "Independent component analysis versus PCA," in *Proceedings of European Signal Processing Conference*, pp. 643–646, Grenoble, France, September 1988.

[9] G. M. Xian, "An identification method of malignant and benign liver tumors from ultrasonography based on GLCM texture features and fuzzy SVM," *Expert Systems with Applications*, vol. 37, no. 10, pp. 6737–6741, 2010.

[10] R. F. Walker, P. T. Jackeay, and I. D. Longstaff, "Recent developments in the use of the Co-occurrence matrix for texture recognition," in *Proceedings of International Conference on Digital Image Processing*, pp. 463–471, Santorini, Greece, July 1997.

[11] L. K. Soh, "Texture analysis of SAR sea ice imagery using gray level Co-occurrence matrices," *IEEE Transactions on*

Geoscience and Remote Sensing, vol. 37, no. 2, pp. 780–795, 1999.

[12] R. Jobanputra and D. A. Clausi, "Preserving boundaries for image texture segmentation using gray level co-occurring probabilities," *Pattern Recognition*, vol. 39, no. 2, pp. 234–245, 2006.

[13] D. A. Clausi, "An analysis of co-occurrence statistics as a function of gray level quantization," *Canadian Journal of Remote Sensing*, vol. 28, no. 1, pp. 45–62, 2002.

[14] P. Philippe, O. Richard, and C. Dubes, "Performance evaluation for four classes of textural features," *Pattern Recognition*, vol. 25, no. 8, pp. 819–833, 1992.